Strain and Temperature Monitoring in Early-Age Concrete by Distributed Optical Fiber Sensing

Carlos G. Berrocal[1,2]([✉]) [iD], Ignasi Fernandez[1] [iD], Ingemar Löfgren[1,2] [iD],
Erik Nordström[3,4] [iD], and Rasmus Rempling[1,5] [iD]

[1] Chalmers University of Technology, 41296 Gothenburg, Sweden
carlos.gil@chalmers.se
[2] Thomas Concrete Group AB, 41254 Gothenburg, Sweden
[3] Vattenfall AB, 16992 Stockholm, Sweden
[4] Kungliga Tekniska Högskolan, 11428 Stockholm, Sweden
[5] NCC AB, 41250 Gothenburg, Sweden

Abstract. In the way towards a carbon neutral construction industry, the partial substitution of cement clinker by alternative binders is becoming increasingly popular in the design of low-carbon concrete mixes. However, as new concrete mixes are developed, the parameters governing the risk of early-age cracking arising from restraint forces due to thermal and shrinkage deformations need to be investigated for each mix. This paper reports the results of a field test in which distributed optical fiber sensors (DOFS) were used to monitor strain and temperature in two large-scale prisms cast against the ground. One of the specimens was cast with a reference concrete mix with CEM I whereas in the other mix cement was partly replaced by fly ash. After casting, mineral wool was used to insulate the specimens in order to reproduce realistic conditions in large mass concrete elements. Temperature measurements enabled a direct comparison of the heat generated by each mix as well as the estimation of the strength development. Strain measurements, on the other hand, gave an indication of the variation of the degree of restraint along the height of the specimens. Using available models for concrete creep, the tensile stresses along the specimens were calculated at different heights and compared to the expected tensile strength in order to assess the crack risk. After removing the insulation, measured strains exhibited a strong dependence on external temperature variations. The test results proved useful to analyse the early-age behaviour of concrete.

Keywords: Early-age concrete · Monitoring · Strain · Temperature · Optical fiber sensors

1 Introduction

Since 2021, the construction works of a new spillway dam in Vattenfall's facility 'Lilla Edet' along the Swedish river Göta älv have been ongoing. For the new dam section, about 8000 m^3 of concrete will be used during construction. The casting of such structures

using mass concrete elements requires a careful control of the heat generated during the hydration of cement in order to minimize the risk of cracking and any eventual durability problems [1].

However, a common trend in Sweden during the last decade has been to reduce the maximum aggregate size and increase the cement content in the concrete mix to improve pumpability and reduce the need for vibration during casting. As a result, today the use of expensive cooling systems with cooling pipes embedded in the concrete is a common solution to mitigate the temperature rise and reduce the risk of cracking at early-age [2, 3].

One of the main goals during the preparation works of the new spillway dam was to substantially reduce the amount of cement in the concrete mix to eliminate the risk of thermal cracking while decreasing the carbon footprint. The target was to completely remove the need for post-cooling and minimize the CO_2 emissions of the concrete mix while fulfilling the requirements on buildability and durability in the harsh Swedish winter climate.

A common way to reduce the amount of cement and heat generation internationally is to use by-products that have pozzolanic properties. To that end, the effect of increasing the maximum aggregate size and replacing cement with different additive materials on temperature development, mechanical properties, frost resistance and sensitivity to carbonation was investigated in several thesis projects [4–6]. Based on the tests results, a low-carbon concrete mix was developed where cement was partially replaced by fly ash from pulverized hard coal power plants [7].

Current regulations, however, limit the amount of cement that can be replaced by mineral additions to retain the strength and durability of concrete at different exposure classes [8]. Moreover, as new mixes are developed, the risk of early-age cracking arising from restraint forces needs to be experimentally investigated for each mix.

The use of DOFS has been gaining traction in the civil engineering field over the last decade due to their multiple advantages over traditional electrical sensors spurring numerous investigations on the applicability of DOFS for the monitoring of RC structures. As a result of those investigations, the suitability of DOFS for strain monitoring and crack detection has been demonstrated experimentally as well as on real on-site applications, see, e.g. [9, 10]. Moreover, recent investigations have shown that DOFS can also be used to assess crack widths and deflections accurately based on distributed strain measurements [11–13]. The applicability of DOFS on the monitoring of RC structures has been, however, mainly focused on the detection and quantification of cracks caused by external loading. Studies exploring the applicability of DOFS to investigate the early-age behavior of concrete and restraint cracking are scarce [14–17].

Consequently, this paper reports the results of a full-scale demonstration casting carried out to determine whether the developed concrete mix performed adequately in practice. The casting had a threefold purpose: (i) to test the pumpability and workability of the concrete with real production apparatus; (ii) to investigate the risk of early-age cracking of the mix in real field conditions; and (iii) to assess the suitability of distributed optical fiber sensing to monitor temperature and strains in a real-scale field test during the curing and hardening of the concrete.

2 Full-Scale Field Tests

2.1 Description of the Specimens

Two concrete mixes with an equivalent water-to-cement ratio of 0.5 were used: a standard concrete with 100% CEM I and a low-carbon concrete with a fly ash to cement ratio of 0.5 (<0.33 according to regulations). A maximum aggregate size of 22 mm was used for the standard mix whereas the maximum aggregate size of the low-carbon mix was increased to 45 mm. The combination of lower cement content and larger aggregate size was expected to yield a reduction of approximately 25–30% in heat development while the carbon footprint was expected to decrease by 20%.

The designed mixes were used to cast two prismatic reinforced concrete specimens in a quarry in Glimmingen, Sweden. The specimens were 6 m long and 1 m wide and were cast against the rock, which provided the main source of external restraint. The specimens were heavily reinforced with both longitudinal and transversal reinforcement consisting of Ø32 bars distributed around the perimeter of a 1 × 1 m square section, as well as Ø32 stirrups distributed along the entire length of the element, with a bar spacing of 100 mm. Figure 1 shows the geometry and reinforcement layout of the specimens.

Immediately after casting, 50 mm thick panels of rock wool were installed around the sides and on top of the specimens increase the temperature in the concrete and to simulate the conditions in a concrete element of representative thickness. The form and rock wool remained for 13 days after which the specimens were demolded.

2.2 Sensor Deployment and Monitoring

In the field tests, both the evolution of temperature over time as well as the development of strains during the hardening period were monitored using a combination of DOFS and vibrating wire strain gauges (VWSG).

In this study, the fiber optic cable BRUsens V1 from Solifos was used, which features an external polymeric protective jacket with rough surface and an outer diameter of 2.8 mm. Unlike other optical fiber sensors commonly used in research, such as the 125 μm-thick polyimide-coated fibers, the V1 cable, thanks to its protective jacket, can be easily handled and deployed without risk of rupture, making it especially suitable for applications in harsh conditions.

Two DOFS were installed in each specimen in a multi-layer configuration, one to monitor strains and another one for temperature. The DOFS used for strain monitoring were fixed to longitudinal reinforcement bars using electric tape and were embedded in the concrete. The DOFS for temperature monitoring were previously inserted into a corrugated plastic tube in order to allow for the free movement of the sensors inside of the specimens. In the specimen cast with the reference concrete mix, the DOFS were installed at four different levels along the vertical symmetry plane of the element whereas in the specimen cast with low-carbon concrete the DOFS were installed at three levels but in two vertical planes, the symmetry plane and a plane close to one of the lateral sides. The position of the DOFS is schematically presented in Fig. 1.
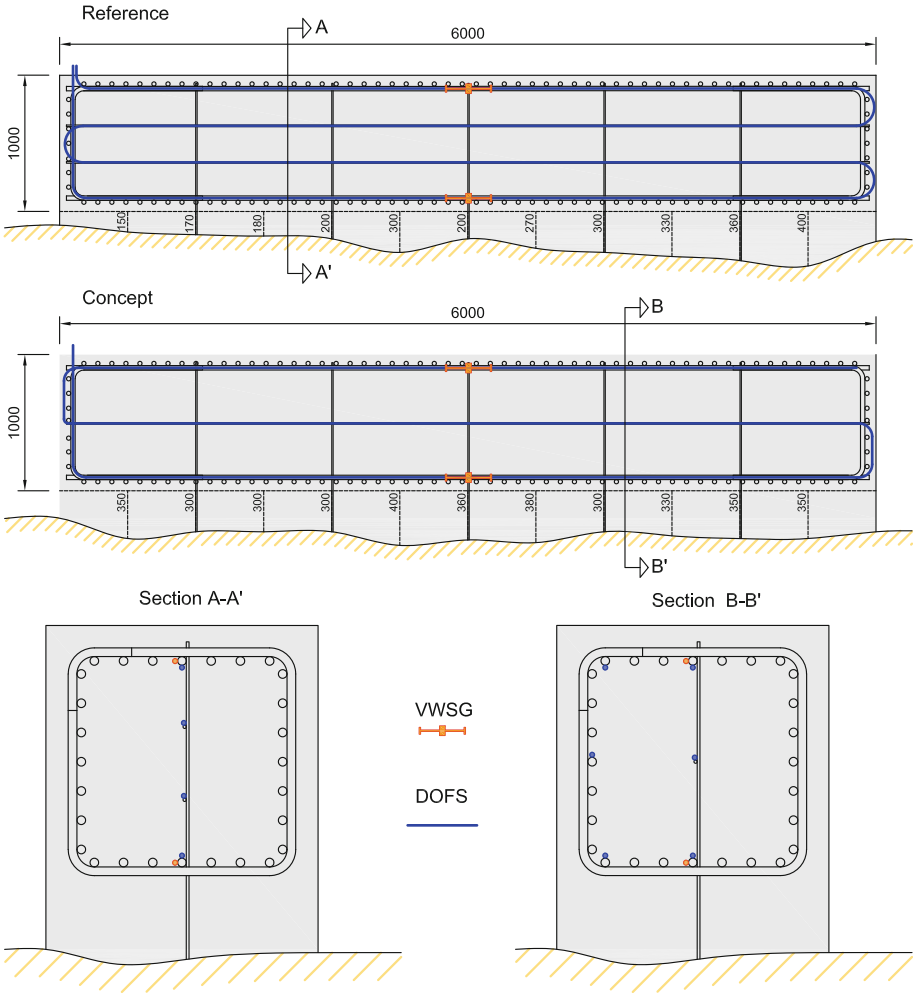
Fig. 1. Geometry of specimens and position of sensors in full-scale specimens

The Optical Distributed Sensor Interrogator (ODiSI) 6000 series from Luna Inc. Was used as data acquisition unit. The ODiSI interrogator offers a strain resolution of 1 με, a maximum strain range of ±15000 με and a sample rate that can go up to 250 Hz. In the tests, a spatial resolution of 2.6 mm was used which provided a combined accuracy (sensor + interrogator) of ±15 με, whereas the sample rate was set to 1 measurement every 10 min.

In order to complement and compare the measurements of the DOFS, two additional VWSG sensors were installed at the top and bottom reinforcement in the mid-section of the specimens. The sensors used were the VWSG model 4200ER from Geokon which has a resolution of 1 με and a measuring range of 10000 με. The sensors are 153 mm long and feature two 20 mm diameter anchorage discs at the ends for effective

embedment in concrete. Moreover, the sensors were equipped with integral thermistors for the simultaneous measurement of temperature.

3 Theory and Method

3.1 Development of Concrete Properties

Maturity Function. Since the rate of cement hydration and hence the development of the mechanical properties of concrete at early-age is affected by temperature, the concept of maturity [18] is used to account such effect. The equivalent time, t_{eq}, based on the Arrhenius equation proposed by Freiesleben Hansen and Pedersen [19] is used according to Eq. (1):

$$t_{eq}(t) = \sum_{i=1}^{t} \exp\left(\theta\left[\frac{1}{T_{ref}} - \frac{1}{T_i + 273}\right]\right) \cdot \Delta t_i \tag{1}$$

where T_i is the average temperature of the concrete in the time interval Δt_i, T_{ref} is a reference temperature usually taken as 20 °C (293 K) and θ is defined as:

$$\theta(T) = \begin{cases} \frac{E_a}{R}\left(\frac{30}{T_i+10}\right)^{\kappa} & for \ T_i > -10°C \\ \infty & for \ T_i \leq -10°C \end{cases} \tag{2}$$

where R is the general gas constant (8.3145 J/K mol), E_a is the activation energy and κ is parameter calibrated experimentally.

Compressive Strength. The expression given by Eqs. (3), (4), which is a slightly modified version of the one included in the Eurocode [20], was used to calculate the development of the compressive strength:

$$f_c(t_e) = f_{cm,28} \cdot \beta(t_e) \tag{3}$$

$$\beta(t_e) = exp\left\{s\left[1 - \left(\frac{672 - t_s}{t_{eq} - ts}\right)^{n_{cc,28}}\right]\right\} \tag{4}$$

where $f_{cm,28}$ is the mean compressive strength in MPa at 28 days determined experimentally for specimens cured at the reference temperature of 20 °C, t_s is the setting time in hours and s and $n_{cc,28}$ are fitting parameters.

Tensile Strength and Modulus of Elasticity. The development of the tensile strength and modulus of elasticity were calculated as suggested by the Eurocode [20], according to Eq. (5) and Eq. (6), respectively:

$$f_{ct}(t_e) = f_{ctm,28} \cdot \beta(t_e) \tag{5}$$

$$E_c(t_e) = E_{cm,28} \cdot \beta(t_e)^{0.3} \tag{6}$$

where $f_{ctm,28}$ is the mean tensile strength in MPa at 28 days determined experimentally for specimens cured at the reference temperature of 20 °C. The mean modulus of elasticity

of concrete at 28 days in GPa, $E_{cm,28}$, is calculated based on the expression given by Eq. (7) as:

$$E_{cm,28} = 22\left(\frac{f_{cm,28}}{10}\right)^{0.3} \tag{7}$$

Creep Coefficient. The variation of total mechanical strain, ε_{tot}, of an element subjected to a constant uniaxial stress, σ, applied at a time t^* can be expressed by Eq. (8) as:

$$\varepsilon_{tot}(t, t^*) = \varepsilon_{el}(t^*) + \varepsilon_{creep}(t, t^*) = \frac{\sigma}{E_c(t_e(t^*))}(1 + \varphi(t, t^*)) \tag{8}$$

where ε_{el} and ε_{creep} are the elastic and creep strains, respectively, and $\varphi(t, t^*)$ is the creep coefficient calculated according to the formulation included in the annex B of the Eurocode [20].

3.2   Determination of Stresses Based on Temperature and Strain Measurements

When a concrete element is cast, the temperature of the concrete will increase due to the heat generated by the cement hydration. When the hydration reaction slows down, the concrete temperature will reach a peak and start descending until it reaches equilibrium with the ambient temperature. During the heating phase, the presence of restraint, either external or internal, will prevent the expansion of the concrete and compressive stresses will arise. Conversely, as the concrete cools down the prevented thermal contraction will give rise to tensile stresses. The time when the first tensile stresses appear in the concrete is denoted, t_2, see Fig. 2.
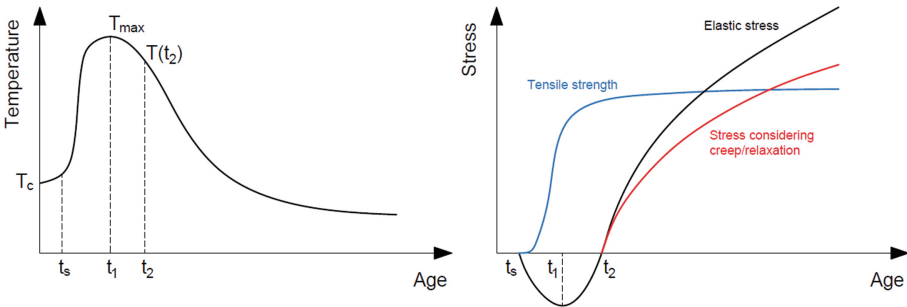

Fig. 2. Typical temperature history of a concrete member (left); tensile strength development and evolution of thermal stresses in a restrained member (right).

Even if the temperature of the concrete after reaching equilibrium with the ambient temperature is similar to the initial temperature of the fresh concrete, T_c, the tensile stresses developed during the cooling phase are greater due to a combination of factors, including a more plastic behaviour in the first hours after casting and the development of the modulus of elasticity of the concrete, which may cause the formation of cracks.

The first step to assess the risk of cracking is to determine the time when tensile stresses arise. The time t_2 corresponds to the moment when thermal contraction after the peak temperature equals the elastic part of the thermal expansion. The corresponding temperature $T(t_2)$ can be found as described in [21] based on Eq. (9):

$$\text{T}(\text{t}_2) = (T_{max} - T_C)\left[1 - \frac{\alpha_{cTe}}{\alpha_{cTc}}(1 - k_0)\right] + T_c \tag{9}$$

where α_{cTe} and α_{cTc} are the concrete thermal expansion coefficients in tension and compression, respectively, and k_0 taken as 0.69 is a factor defining the proportion of plastic strain during the heating phase. The time t_2 can then be determined from the temperature history, after which the mechanical tensile strain, $\varepsilon_t(t)$, can be calculated as:

$$\varepsilon_t(t) = [\varepsilon_{mes}(t) - \varepsilon_{mes}(t_2)] - \alpha_{cTe}[T(t) - T(t_2)] \tag{10}$$

where ε_{mes} is the total strain measured by the sensors. Finally, the tensile stress developed at an arbitrary time $t_n > t_2$ can be computed by adding the contribution of the incremental strain change in each time step as:

$$\sigma(t_n) = \sum_{t_i} \Delta\varepsilon_{t,i}\cdot\frac{E_c(t_e(t_i))}{1 + \varphi(t_n, t_i)} \quad for\ t_i = t_2 + \Delta t, \dots, t_n \tag{11}$$

where $\Delta\varepsilon_{t,i} = \varepsilon_t(t_i) - \varepsilon_t(t_{i-1})$ is the incremental change of mechanical tensile strain at the *i-th* time step and Δt is the time increment between time steps. It should be noted that the effect of shrinkage, neither autogenous nor drying shrinkage has been considered in this study. While it has been shown that the contribution of drying shrinkage for this type of elements is small, especially at very early ages [22], autogenous shrinkage may in certain cases have a significant impact on the tensile strain and should therefore be generally considered.

4 Results and Discussion

An example of the data measured with the DOFS is shown in Fig. 3 for both the evolution of temperature and strain along the sensor positioned along the top reinforcement bar of the reference specimens. As observed, this measurement technique enables a detailed description of temperature and strain in both time and space. Moreover, it can be observed that whereas the measured temperatures display a smoother signal, the strain measurements are heavily influenced by the heterogeneities of the concrete, indicating that the actual distribution of strains in the concrete is far from the idealized uniform behavior.

In Fig. 4, the temperature history at the top and bottom reinforcement of the midsection is compared for the reference and low-carbon concrete specimens. As observed, the results show that the maximum temperature in the reference concrete reached 50.4 °C and 44.2 °C at the top and bottom reinforcement, respectively. For the low-carbon concrete, the maximum measured temperature in the same positions was 41 °C and 33.4 °C respectively. These values mean a reduction of the maximum temperature in the concrete
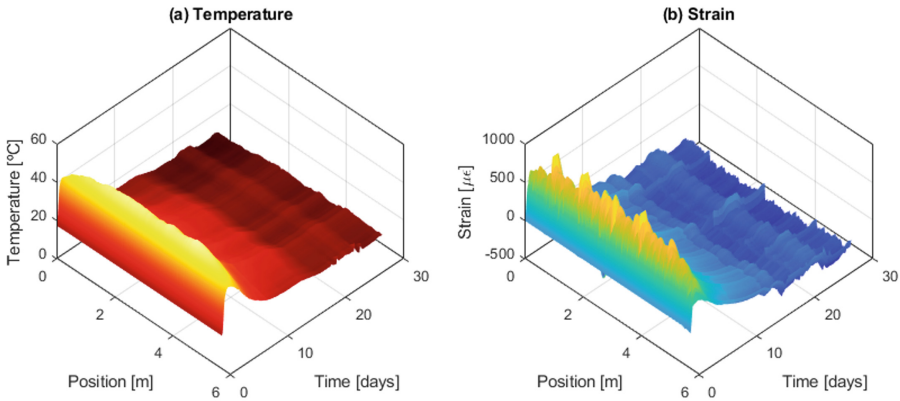
Fig. 3. Example of experimental measurements obtained with the DOFS for (a) temperature and (b) strain, for the sensors located at the top reinforcement bar in the reference specimen.

of approximately 19% and 24%, indicating that designed low-carbon concrete mix could be used to effectively reduce the need for cooling in the real dam.

Figure 4 also reveals that the maximum temperature of the concrete at the bottom side of the specimens reached a somewhat lower value due to the boundary effect of the soil, which was likely significantly colder as the measurements were carried out in the month of November. Conversely, after removing the form and the insulation, the temperature in the top side of the specimens displayed a strong dependence on the ambient temperature while the temperature in the bottom exhibited smoother variations.
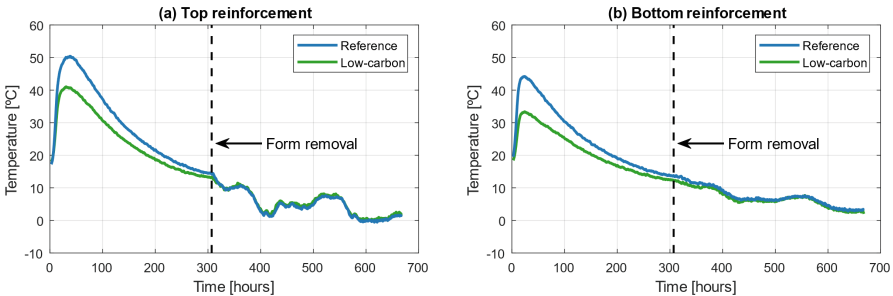

Fig. 4. Comparison of temperature development between the reference and low-carbon concrete specimens at (a) the top reinforcement and (b) the bottom reinforcement.

Based on the method described in Sect. 3, strain measurements can provide additional insight into the risk of cracking. The input values for the different parameters used to calculate the development of the concrete properties and stress buildup are summarized in Table 1.

In Fig. 5, the measured strains are compared to the calculated thermal strains caused by the temperature change in the concrete at the location of the top and bottom reinforcement. From Fig. 5, it can be observed that as time proceeds, a certain change in thermal strain produces a lower response in the corresponding measured strain, which can be explain by an increase of the degree of restraint due to a higher modulus of elasticity of the concrete over time.

Table 1. Parameters used for crack risk analysis

| Parameter	Reference mix	Low-carbon mix
Activation Energy, E_a [J/mol]	29900	34900
Activation energy exponent, κ, [−]	0.219	0.4
Mean compressive strength at 28 days, $f_{cm,28}$, [MPa]	42.6	42.6
Compressive strength shape parameter, s [−]	0.25	0.69
Setting time, t_s, [hours]	9.32	9.5
Compressive strength exponent, $n_{cc,28}$, [−]	0.56	0.31
Mean tensile strength at 28 days, $f_{ctm,28}$, [MPa]	3.26	3.26
Relative humidity, RH, [%]	80	80
Notional member size, h_0, [mm]	667	667
Thermal coefficient of expansion, α_{cTe} [°C^{-1}]	$10 \cdot 10^{-6}$	$10 \cdot 10^{-6}$
Thermal coefficient of contraction, α_{cTc}, [°C^{-1}]	$7.6 \cdot 10^{-6}$	$7.6 \cdot 10^{-6}$
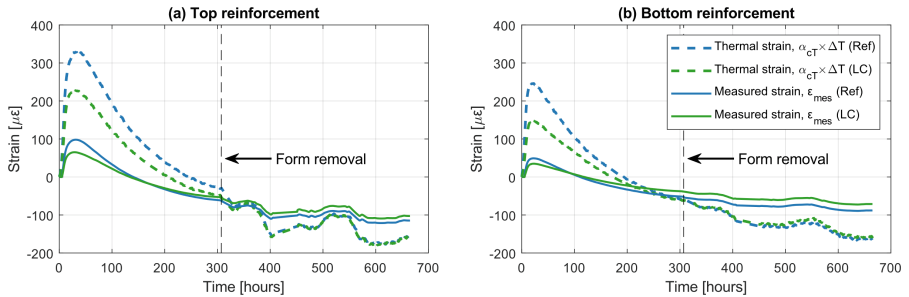
Fig. 5. Comparison of the calculated thermal strains and measured strains by the DOFS for the reference and low-carbon specimens at the (a) top reinforcement and (b) bottom reinforcement.

Finally, an estimation of the cracking risk is presented in Fig. 6 as the relation between the calculated tensile stress growth in the concrete specimens and the development of the tensile strength. The results shown in Fig. 6 correspond to the position of the top reinforcement since this was the part of the specimens that reached the highest measured temperature.

It can be observed in Fig. 6 that even though the development of the tensile strength occurred slightly more slowly for the low-carbon mix, the low-carbon specimen displayed a significantly lower stress to strength ratio, which after 28 days was 0.67 compared to 0.84 for the reference specimen. This is attributed to the reduction of the peak temperature which resulted in a lower thermal contraction in the cooling phase combined with a slower development of the modulus of elasticity.

It is worth noting that after the removal of the formwork, the risk of cracking is strongly dependent on the ambient temperature, where large negative thermal gradients, i.e., a significant reduction of the air temperature over a short period of time, yielded noticeable spikes of the buildup stress, see, e.g. Fig. 6 at approximately 400 h. Moreover, Fig. 6 also shows the impact of including the effect of creep in the stress calculation, which highlights the importance of characterizing the tensile creep of concrete to assess the risk of cracking accurately.
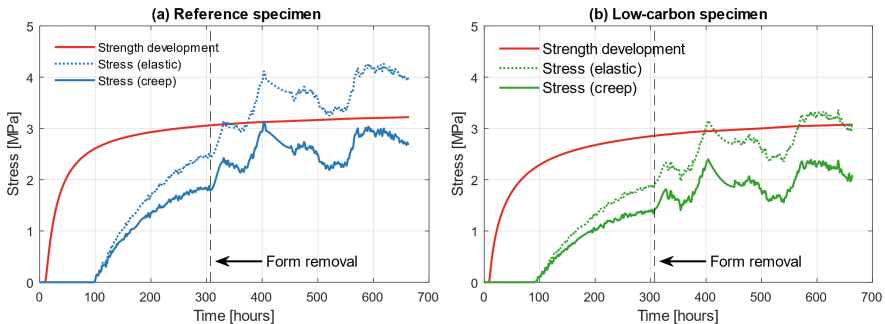

Fig. 6. Evaluation of the crack risk at the position of the top reinforcement for (a) the reference specimen and (b) the low-carbon specimen.

5   Conclusions

This paper presented the results of a full-scale field test where distributed optical fiber sensors based on Rayleigh backscattering were used to assess the heat development and crack risk of a low-carbon concrete mix for the upcoming construction of a spillway dam in Sweden. The distributed sensing technology used enabled the simultaneous measurement of temperature and strain along the entire length of the specimens at different levels using only two cables per specimen. This shows a great potential for the early-age monitoring of large mass concrete elements. The temperature measurements revealed that the final mix design with increased maximum aggregate size and partial replacement of cement by pulverized fly ash, not only resulted in a climate enhanced concrete but it also yielded a reduction of the peak temperature ranging between 19% and 24%. The measured temperature history was used to calculate the development of the concrete mechanical properties based on the maturity method and preliminary laboratory tests. Using the strain measurements, the tensile stress in the concrete was estimated

including the effect of creep based on existing calculation models. Due to the lower temperature reached in the low-concrete mix, the risk of cracking was significantly reduced, eliminating the need for a post-cooling system and resulting in important economical savings.

References

1. Bamforth, P.B.: Early-age thermal crack control in concrete (2007)
2. Bernander, S., Emborg, M.: Temperaturförhållanden och sprickbegränsning i grova betongkonstruktion. In: Betonghandbok, Svensk Byggtjänst och Cementa AB, Stockholm (1992)
3. Petersons, N.: Sprickor. In: Betonghandbok, Svensk Byggtjänts och Cementa AB, Stockholm (1994)
4. Bohlin, K.: Snibb RKarbonatisering av slagg- och flygaskebetong - och dess inverkan på transportegenskaper (2016)
5. Lagundžija, S.: Thiam MTemperature reduction during concrete hydration in massive structures (2017)
6. Barchin, A.: Sedighi NAlternative methods to prevent thermal cracking in concrete (2019)
7. Nordström, E.: Temperaturrelaterade sprickor i vattenbyggnadsbetong – alternativa metoder för riskreduktion. Stockholm, KTH Betongbyggnad, report Num. TRITA-ABE-RPT-1910 (2019)
8. Svenska Institutet för Standarder. SS 137003:2021 Concrete - Application of SS-EN 206:2013+A2:2021 in Sweden (2021)
9. Berrocal, C.G., Fernandez, I., Rempling, R.: Crack monitoring in reinforced concrete beams by distributed optical fiber sensors. Struct. Infrastruct. Eng. **17**, 124–139 (2021)
10. Barrias, A., Rodriguez, G., Casas, J.R., Villalba, S.: Application of distributed optical fiber sensors for the health monitoring of two real structures in Barcelona. Struct. Infrastruct. Eng. **14**, 967–985 (2018)
11. Fernandez, I., Berrocal, C.G., Rempling, R.: Long-term performance of distributed optical fiber sensors embedded in reinforced concrete beams under sustained deflection and cyclic loading. Sensors **21**, 6338 (2021)
12. Fernandez, I., Berrocal, C.G., Almfeldt, S., Rempling, R.: Monitoring of new and existing stainless-steel reinforced concrete structures by clad distributed optical fibre sensing. Struct. Health Monit. 147592172210811 (2022)
13. Brault, A., Hoult, N.: Monitoring reinforced concrete serviceability performance using fiber-optic sensors. ACI Struct. J. **116**, 57–70 (2019)
14. Liu, L., Huang, D., Wang, Z., Xin, J., Liu, Y.: Estimation of thermal stresses in the field test under the restraint method. Constr. Build. Mater. **229**, 116890 (2019)
15. Ouyang, J., Chen, X., Huangfu, Z., Lu, C., Huang, D., Li, Y.: Application of distributed temperature sensing for cracking control of mass concrete. Constr. Build. Mater. **197**, 778–791 (2019)
16. Bado, M.F., et al.: Characterization of concrete shrinkage induced strains in internally-restrained RC structures by distributed optical fiber sensing. Cem. Concr. Compos. **120**, 104058 (2021)
17. Oukhemanou, E., Desforges, S., Buchoud, E., Michel-Ponnelle, S., Curtois, A.: VeRCoRs Mock-Up: Comprehensive monitoring system for reduced scale containment model. In: 3rd Conference on Technological Innovations in Nuclear Civil Engineering, SFEN, Paris (2016)
18. Chengfu, G.: Maturity of concrete: Method for predicting early-stage strength. ACI Mater. J. **86**, 341–353 (1989)

19. Freiesleben Hansen, P., Pedersen, E.J.: Måleinstrument til control af betons hærdning ("Maturity Computer for Controlled Curing and Hardening of Concrete"). Nordisk Betong. **1**, 21–25 (1977)
20. EN 1992-1-1 Eurocode 2EN 1992-1-1 Eurocode 2: Design of concrete structures - Part 1-1: General rules and rules for buildings (2004)
21. Engström, B.: Restraint cracking of reinforced concrete structures. Undervisningmaterial Institutionen för bygg- & miljöteknik, Chalmers tekniska högskola (2006)
22. Smolana, A., Klemczak, B., Azenha, M., Schlicke, D.: Thermo-mechanical analysis of mass concrete foundation slabs at early age—essential aspects and experiences from the FE modelling. Materials **15**, 1815 (2022)